A CRISPR screen identifies UFMylation and TRAMP-like complexes required for hepatitis A virus infection

Jessie Kulsuptrakul[1], Ruofan Wang[1], Nathan L. Meyers[2], Melanie Ott[2], Andreas S. Puschnik[1]

[1] Chan Zuckerberg Biohub, San Francisco, United States

[2] Gladstone Institutes, University of California San Francisco, San Francisco, United States

Correspondence to: andreas.puschnik@czbiohub.org

Abstract

Hepatitis A virus (HAV) is a single-stranded, positive-sense RNA virus and a hepatotropic member of the *Picornaviridae*. Despite successes in vaccine development, HAV remains a common cause of enterically transmitted hepatitis globally, responsible for epidemics in developing and developed countries with symptoms ranging from mild inflammation and jaundice to acute liver failure[1,2]. A comprehensive picture of the cellular factors, which are co-opted by HAV to replicate and establish successful infection, is missing. Here, using a genome-scale CRISPR screen in a human hepatocyte cell line, we identified genes involved in sialic acid and ganglioside biosynthesis, the eukaryotic initiation factor complex and the endosomal sorting complexes required for transport (ESCRT), which have known roles in viral pathogenesis[3–12]. Additionally, we uncovered host factors not previously linked to HAV infection. We found all components of the cellular machinery for UFMylation, a ubiquitin-like protein modification[13], and showed that optimal translation of the HAV genome depends on functional UFM1 conjugation in host cells. Furthermore, we identified PAPD5, PAPD7 and ZCCHC14, which form a complex related to the yeast Trf4/5–Air1/2–Mtr4 polyadenylation (TRAMP) complex[14]. We demonstrated that loss of the TRAMP-like complex directly results in reduced viral translation efficiency, without affecting HAV poly(A) tails. Finally, we showed that pharmacological inhibition of PAPD5 and PAPD7 decreased HAV replication in hepatocyte cells as well as human liver organoids. Thus, our study revealed novel cellular pathways, specifically important for HAV translation, and provided a new strategy for host-directed therapy of severe HAV infection.

Main

Viruses are obligate intracellular pathogens that depend on host cell components for replication. HAV enters host cells through interactions with cell surface molecules, followed by uncoating and delivery of viral RNA from endosomes to the cytosol. The viral polyprotein is synthesized under the control of an internal ribosome entry site (IRES) and processed into the individual structural and non-structural proteins. HAV co-opts cellular membranes to form organelle-like structures, where viral genome replication occurs. The newly synthesized genomes are packaged and HAV egresses in form of quasi-enveloped virions. Despite a general understanding of the life cycle[15], a comprehensive overview of the most critical host factors for HAV infection is lacking. CRISPR screens are a powerful technology to interrogate cell components critical for viral infection in an

unbiased fashion, which provides insights into the molecular host-pathogen interactions and may reveal suitable targets for host-directed therapies[16].

To identify host cellular factors that are critical for HAV infection, we conducted a genome-wide CRISPR knockout (KO) screen in the human hepatocyte cell line Huh7.5.1 using the cytopathic HAV HM175/18f strain (Fig. 1a). Infection led to notable cell death after ~3 days and surviving cells were collected after 12 days for analysis. We consistently found enrichment of guide RNA (gRNA) sequences targeting genes involved in several pathways known to be required for picornaviral replication (Fig. 1b, Supplementary Fig. 1a, Supplementary Table 1). For example, sialic acid and ganglioside biosynthesis (*GNE, CMAS, SLC35A1, UGCG, ST3GAL5*), which were previously implicated in entry of picorna- and other viruses[3–6]. We also identified *PTBP1* and members of the eukaryotic initiation factor complex (*EIF4B, EIF3C, EIF3CL*), which have known roles in IRES-mediated translation of HAV and other picornaviruses[7–10]. VPS4A is an ESCRT component, important for budding of several enveloped viruses as well as egress of HAV[11,12]. Identification of these genes known to be important for HAV or viral pathogenesis in general highlights the robustness of this genetic screen. Importantly, gene ontology (GO) analysis of enriched genes (RIGER p-value < 0.001) revealed additional pathways, which have not previously been implicated in HAV infection, such as the machinery for UFMylation (*UFM1, UBA5, UFL1, UFC1, UFSP2*), a ubiquitin-like protein modification[17], and the TRAMP complex components PAPD5 (also known as TENT4B or TRF4-2) and PAPD7 (also known as TENT4A or TRF4-1) (Fig. 1b,c and Supplementary Table 2)[18]. Zinc Finger CCHC Domain-Containing Protein 14 (ZCCHC14), which has been shown to associate with PAPD7 using BioID, is likely to be part of a TRAMP-like complex, which generally contains a zinc knuckle protein[19,20].

We systematically compared our hits with CRISPR screens for host factors of human rhinovirus C15 (HRV-C15) and enterovirus D68 (EV-D68), two other *Picornaviridae* members[21]. Other than sialic acid biosynthesis genes among the EV-D68 hits, there were no commonalities, indicating divergent evolution of host factor dependence between HAV and these distantly related picornaviruses (Supplementary Fig. 1b,c). Additionally, we compared our results to a CRISPR screen for hepatitis C virus (HCV) infection, another hepatotropic positive-sense RNA virus (and member of the *Flaviviridae* family) but found no overlap in the host factor requirements (Supplementary Fig. 1d)[22].

To validate the results of our screen, we generated isogenic KO cell lines in several genes using CRISPR-Cas9 gene editing (Supplementary Fig. 2a). Upon HAV infection, we observed significant reduction of viral RNA (ranging from 10-1,000 fold) relative to levels in wild-type (WT) cells at 72 hours post-infection (hpi) (Fig. 1d). As PAPD5 and PAPD7 are both human orthologues of yeast Trf4p and display redundancy in their polyadenylation function[18], we generated *PAPD5/PAPD7* double knockout (DKO) cell lines (Supplementary Fig. 2b). We observed a significantly stronger reduction in viral replication in the DKO cells compared to the single *PAPD5* or *PAPD7* KO cells underscoring their redundant activity for HAV replication (Fig. 1e). Next, we

performed a timecourse infection assay using a recombinant reporter virus that expresses nanoluciferase from within its polyprotein (HAV-NLuc). We measured a ~10^4 fold increase in luminescence in WT cells after 72hpi but there was striking attenuation of luciferase expression in host factor KO lines (Fig. 1f). Moreover, when we complemented *UBA5*, *PAPD5* and *ZCCHC14* KO cells with the respective cDNAs, we observed a significant increase in HAV RNA levels (Fig. 1g-i). To rule out that phenotypes are not only observed with the highly tissue culture adapted HM175/18f strain, we additionally performed infection assays in KO cell lines using a low-passage HM175 strain with similar results (Supplementary Fig. 3).

Next, we compared replication of different *Picornaviridae* members in *UFM1* KO cells (Supplementary Fig. 2c). As expected, HAV RNA levels were greatly reduced while enterovirus 71 (EV-71) and encephalomyocarditis virus (EMCV) RNA levels were not affected (Fig. 1j). Interestingly, human rhinovirus A2 (RV-A2) replication was significantly increased suggesting that UFMylation can mediate pro- and antiviral functions in host cells, depending on the virus species. In cells deficient in both PAPD5 and PAPD7, HAV RNA levels were severely and EMCV RNA levels moderately decreased while EV-71 and RV-A2 replication was unaffected (Fig. 1k).

It is of note that our screen did not reveal HAVCR1 (also known as TIM1) as an essential host factor for HAV infection. HAVCR1 was originally identified as a HAV receptor but a more recent study questioned its essentiality for HAV infection[23,24]. To address this further, we generated isogenic *HAVCR1* KO lines and performed a viral attachment and internalization assay (Supplementary Fig. 4). We only observed a minor defect of internalized virions at 6hpi and viral RNA levels were only reduced by ~2 fold relative to WT cells at 30hpi (Supplementary Fig. 4). Thus, *HAVCR1* KO cells were unlikely to be protected against cytopathic HAV infection in the CRISPR screen. By contrast, in *SLC35A1* KO cells intracellular viral RNA was decreased by ~80% at 6hpi and ~95% at 30hpi (Supplementary Fig. 4). We conclude that *HAVCR1* is not essential for the HAV life cycle, while sialic acid biosynthesis is critical for viral entry and establishing infection. Together, these data confirm that the genes identified by the CRISPR screen play an important role in the HAV life cycle.

UFM1 encodes the 85 amino acid long ubiquitin-fold modifier 1, which acts as a protein modification and is conserved among most eukaryotes except for yeast and other fungi[13]. Like ubiquitination, UFM1 is covalently attached to its targets following an E1–E2–E3 reaction consisting of the UFM1-activating enzyme UBA5, the UFM1-conjugating enzyme UFC1 and the UFM1-specific ligase UFL1 (Fig. 2a)[13,25]. Usually, UFM1 is present in a precursor form, which first requires cleavage of the last two C-terminal amino acids by the UFM1-specific protease UFSP2 to expose Gly at position 83 (ref. [13]). UFSP2 also operates as the major de-UFMylation enzyme, removing UFM1 molecules from their targets[26]. Our screen identified all known components of the UFMylation machinery including the additionally associated proteins DDRGK1 and ODR4 (encoded by *C1orf27*) (Fig. 2a, Supplementary Table 1)[27,28]. To date, this protein modification has

not been implicated to play a role in viral infections. WT cells contain free UFM1 as well as conjugated UFM1 as detected by immunoblot (Fig. 2b). To probe whether functional conjugation of UFM1 is required for HAV infection, we mutated different components of the pathway. Deletion of UBA5 led to an absence of conjugated UFM1, while UFSP2 KO resulted in hyper-conjugation (Fig. 2b). However, both conditions led to a stark reduction of viral RNA in infected cells (Fig. 2c). Moreover, we generated cell lines either lacking UFM1 completely or expressing WT UFM1, Gly83Ala UFM1 or ΔC3 UFM1 (lacking the last 3 C-terminal amino acids) and showed the presence of conjugated UFM1 in cells containing WT UFM1, hyper-conjugation with Gly83Ala UFM1 and absence of UFM1 linkage for ΔC3 UFM1 consistent with previous findings (Fig. 2b)[13]. Complementation with WT UFM1 significantly restored HAV replication, although less than the hyper-conjugated Gly83Ala UFM1, possibly because the Gly83Ala mutant may be more stable due to resistance to UFM1 processing (Fig. 2c). By contrast, conjugation-deficient ΔC3 UFM1 did not rescue viral infection indicating that functional UFM1 conjugation is indeed critical for HAV (Fig. 2c). Complementation of *UBA5* KO cells with WT UBA5 but not catalytically inactive enzyme also restored UFM1 conjugation and viral replication (Fig. 2b, Supplementary Fig. 5a,b).

Next, we used HAV replicon RNA expressing firefly luciferase to assess whether the defect occurs during the viral translation or genome replication step and detected a moderate defect in *UBA5* and *UFM1* KO cells within 10h post-electroporation, which further increased at later timepoints (Fig. 2d). To specifically measure the effect on translation of incoming viral RNA, we additionally used a replication-incompetent replicon (containing a GDD→GAA mutation in the viral polymerase) and observed a greater than 2-fold decrease of luciferase expression in both *UBA5* and *UFM1* KO cells (Fig. 2e). Thus, we conclude that functional conjugation of UFM1 is required for efficient translation of HAV RNA.

PAPD5 and PAPD7 are two non-canonical poly(A) RNA polymerases (ncPAPs), which can transfer oligo(A) to a variety of RNA substrates (including mRNAs, miRNAs, snoRNAs and rRNAs) in a template-independent manner[29–33]. Their activities have been shown to stabilize mRNAs for translation as well as to specify different RNA species for turnover by the exosome complex[14,18,34]. ZCCHC14 has been implicated to interact with these ncPAPs forming a TRAMP-like complex[19,35]. We measured the effects of either *PAPD5/7* DKO or *ZCCHC14* KO on viral translation and replication using viral replicon RNA and observed a notable defect early post-electroporation before the onset of viral genome replication (Fig. 3a). While we detected low levels of replication between 24 and 32h in the host factor KO cell lines, luminescence dropped to near background levels by 48h. We determined that the catalytic activities of PAPD5 and PAPD7 are likely to be required to support viral infection as complementation of KO or DKO cells with WT PAPD5 or PAPD7 but not catalytically inactive (CAT) PAPD5 or PAPD7 (containing two aspartate to alanine substitutions in the active site) restored HAV replication (Supplementary Fig. 6a-c)[29]. PAPD5 and PAPD7 can regulate the length of poly(A) tails of certain mRNAs, which can affect RNA stability

and translation. As HAV has a polyadenylated genome, we assessed the length of viral poly(A) tails from infected WT and DKO cells by polyacrylamide gel electrophoresis but we did not observe a difference (Fig. 3b). We additionally analyzed the poly(A) tails by TOPO cloning and Sanger sequencing with similar results (Fig. 3c). Recently, it was shown that PAPD5 and PAPD7 can introduce guanosines at low frequencies into poly(A) tails resulting in increased stability against CCR4-NOT dependent deadenylation and prolonged mRNA half lives[36]. However, we did not observe an elevated frequency of non-adenosine nucleotides in WT vs DKO cells within HAV poly(A) tails (Fig. 3e, Supplementary Table 3). Rather, almost all tails exclusively consisted of adenosines. In addition to the absence of changes in HAV poly(A) tail length or composition, we did not detect differences in overall viral RNA stability between WT, DKO as well as *ZCCHC14* KO cells early post viral entry (2-8h), suggesting that HAV RNA is fairly stable even in absence of TRAMP components (Fig. 3e). Finally, we probed viral translation directly using the replication-incompetent HAV replicon and observed drastically reduced luciferase levels in the first 10h post-electroporation in DKO and *ZCCHC14* KO cells, consistent with the WT replicon data (Fig. 3f). By contrast, translation of electroporated firefly mRNA was not affected (Supplementary Fig. 7a). Additionally, we ruled out effects on the poly(A) tails of *in-vitro* transcribed and electroporated replicon RNA containing a defined stretch of 40 adenosines (Supplementary Fig. 7b). Therefore, we propose a critical role of the TRAMP-like complex in facilitating HAV translation in a poly(A) tail length and stability-independent manner.

Next, we sought to explore whether pharmacological inhibition of PAPD5/7 exhibits an antiviral effect on HAV replication. We used RG7834 (Fig. 4a), a small molecule compound belonging to the chemical class of the dihydroquinolizinones, which was first identified as a potent inhibitor for hepatitis B virus (HBV) surface antigen (HBsAg) secretion[37]. Additional studies using yeast three-hybrid screening identified PAPD5 and PAPD7 as the cellular targets for RG7834[38]. We performed a dose-response curve and calculated a 50% effective concentration (EC_{50}) of 12.76nM for inhibition of HAV replication, which is far below the reported 50% cytotoxic concentration (CC_{50}) of >10 µM and consistent with our measurements (Fig. 4b, Supplementary Fig. 8a)[37]. Drug treatment of infected *PAPD5* or *PAPD7* KO cells suggested that RG7834 has a stronger inhibitory effect on the PAPD5 activity as reduction of viral RNA is more substantial in the *PAPD7* KO+RG7834 condition (Supplementary Fig. 8b). Intrigued by the fact that RG7834 inhibits both HAV and HBV, we also measured the effects on two additional liver-specific viruses, HCV and hepatitis E virus (HEV). However, RG7834 only showed significant reduction of HAV and HBV RNA levels (Fig. 4c-f). This is consistent with unchanged viral replication levels of HCV and HEV in DKO cells (Supplementary Fig. 8c). Finally, we performed infection assays in human liver organoid cultures[39]. Both stem cell-like and differentiated organoids were infected with HAV and treated with 100nM RG7834. In both organoid conditions, we observed significant reduction of

HAV RNA (Fig. 4g,h), highlighting that pharmacological targeting of PAPD5/7 is a promising strategy for host-directed therapy of HAV infection.

Discussion

This study provides a comprehensive assessment of the host factors that are required for HAV infection. We reveal two cellular pathways, UFMylation and a TRAMP-like complex, which had not been implicated in HAV replication before. We demonstrated that UFMylation is required for HAV translation in a UFM1-conjugation dependent manner. The cellular function of this protein modification is still an emerging field of research. Recently, the Ribosomal Protein L26 (RPL26) was identified as a major target for UFMylation in human cells and linked to a role in ER-localized ribosome-associated quality control[40,41]. Specific ribosomal or ribosome-associated proteins have been shown to be required for efficient IRES-mediated translation of viral genomes but whether HAV translation depends on ribosomes containing ufmylated RPL26 warrants further investigation[42,43]. In general, UFMylation has been linked to the regulation of ER stress response and autophagy and it is possible that HAV is vulnerable to perturbations of the cellular protein homeostasis[17]. Interestingly, our results indicate that both hypo- and hyperconjugation of UFM1 is suboptimal for HAV infection. By contrast, we found that deletion of *UFM1* led to a substantial increase of RV-A2 infection, suggesting that UFMylation can also mediate antiviral functions in host cells. Thus, the contrasting phenotypes of HAV and RV-A2 replication in response to *UFM1* KO can be utilized as molecular tools for future studies of the effects of UFMylation on viral pathogenesis as well as cellular processes in general.

Furthermore, we identified ZCCHC14 together with PAPD5 and PAPD7, two ncPAPs, which have been shown to be the catalytic subunit of a TRAMP-like complex involved in post-transcriptional quality control mechanism[14]. In context of the nuclear TRAMP machinery, PAPD5/7 interact with ZCCHC7, another CCHC-motif containing zinc knuckle protein, and the Mtr4 exosome RNA helicase (MTREX/SKIV2L2), which were both not enriched in the HAV CRISPR screen. This suggests that PAPD5/7 can form different complexes with specific cellular activities, for example template-independent polyadenylation of its nuclear RNA substrates with short oligo(A) tails for targeted degradation by the exosome or increase of mRNA stability by poly(A) tail extension or mixed tailing[18,44]. We demonstrated that the pro-viral function of the identified TRAMP-like complex is important for the translatability of HAV RNA, independent from modifying its poly(A) tails. This is consistent with previous observations that picornavirus polyadenylation is template-dependent, for example by the presence of a homotypic poly(U) sequence in the picornavirus negative-sense RNA[45]. Moreover, studies using poliovirus, another picornavirus, suggested that the picornaviral RNA-dependent RNA polymerase use reiterative transcription as it replicates the poly(A) tails of viral RNA[46,47]. These findings support that ncPAPs are not required for HAV poly(A) tail generation or maintenance. In studies using *C. elegans*, deletion of the worm orthologs of PAPD5 (gld-4) and ZCCHC14 (gls-1) led to reduced polysome formation but did not

affect global poly(A) tail lengths providing evidence of polyadenylation-independent functions of TRAMP-like complexes[48]. The utilization and re-purposing of cellular RNA-binding proteins to enhance translation or other steps in the viral life cycle is a commonly used strategy by positive-sense RNA viruses[49,50]. Unexpectedly, we found that mutations in the active sites of PAPD5/7 affected HAV infection. It is possible that the catalytic mutations have structural implications and impair the co-opted non-catalytic activity (as suggested by reduced protein levels of the catalytic mutant by immunoblot). Alternatively, PAPD5 and PAPD7 may affect stable expression or turnover of another host factor critical to HAV translation through RNA tailing.

Interestingly, other tested picornaviruses were not dependent on the TRAMP-like complex for efficient translation despite commonalities in their gene expression strategy. Surprisingly though, PAPD5, PAPD7 and ZCCHC14 were identified as critical factors for HBV infection in chemical and CRISPR screens[35,38]. HBV is a chronic, hepatotropic DNA virus, which replicates through reverse transcription, uses host RNA polymerase II for the transcription of viral mRNAs and initiates translation independent of an IRES[51,52]. Mechanistically, it was shown that the TRAMP-like complex played an important role in HBsAg expression by poly(A) tail extension of HBsAg mRNAs[35]. Together, this highlights a remarkable convergence of two unrelated hepatitis viruses to co-opt the same cellular complex through different molecular functions.

Finally, we provided proof-of-concept that pharmacological inhibition of PAPD5/7 decreases HAV (as well as HBV) levels. Fulminant hepatitis is a rare but severe complication of HAV infection, which can result in liver transplantation or death. As current treatment is largely supportive, inhibition of PAPD5/7 may thus be a new strategy for host-directed therapy in cases of fulminant hepatitis. Overall, this study provides a comprehensive picture of HAV host factors. In addition to the eukaryotic initiation factor complex and PTBP1 known to be required for HAV translation, we uncovered UFMylation and the TRAMP-like complex, thus highlighting a complex interplay of HAV with its host cell to achieve successful viral protein biogenesis.

Figures

Figure1

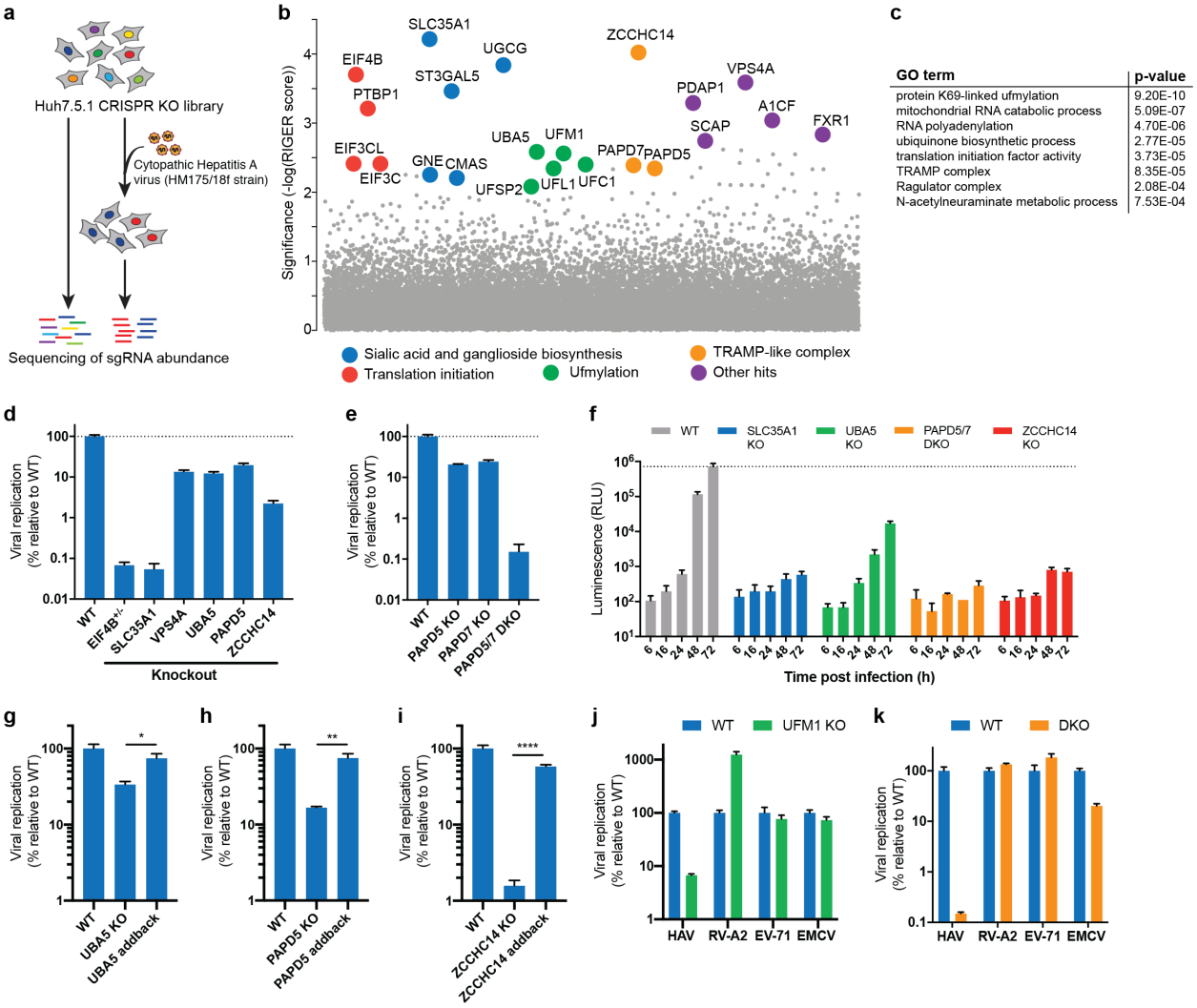

Fig. 1: Genome-wide CRISPR KO screen identifies host cellular factors important for HAV infection. a, Schematic of the genome-wide CRISPR KO screening setup. A library of Huh7.5.1 CRISPR-Cas9 cells was infected with cytopathic HAV HM175/18f and virus-resistant cells were harvested 12 days post-infection (dpi). gRNA abundance was assessed in the original and selected cell population by next-generation sequencing. **b,** Plot of RIGER analysis to calculate the significance of enriched genes in CRISPR KO screen. Certain enriched genes were clustered and colored by function. **c,** Selected terms from gene ontology (GO) analysis of genes enriched in CRISPR KO screen (RIGER p-value < 0.001). **d,** Quantification of HAV RNA in WT and clonal KO cell lines 3 dpi by RT-qPCR. Dotted line indicates 100% infection levels in WT cells. **e,** Quantification of HAV RNA in WT, *PAPD5* KO, *PAPD7* KO and *PAPD5/PAPD7* double KO (DKO) cells 3 dpi by RT-qPCR. **f,** Viral growth curves using recombinant HAV expressing nanoluciferase (HAV-Nluc). WT, *SLC35A1* KO, *UBA5* KO, *PAPD5/7* DKO and *ZCCHC14* KO cells were infected, lysed at indicated timepoints and luciferase levels were measured. Dotted line indicates luminescence levels in WT

cells at 72 hpi. Data are displayed as means ± s.d. (n=2 biological replicates). **g-i,** Quantification of HAV RNA in WT, *UBA5* KO (**g**), *PAPD5* KO (**h**), or *ZCCHC14* KO (**i**) cells and KO cells complemented with respective cDNAs 3 dpi by RT-qPCR. **j-k,** Quantification of HAV, human rhinovirus A2 (RV-A2), enterovirus 71 (EV-71) and encephalomyocarditis virus (EMCV) RNA in WT vs *UFM1* KO cells (**j**) or WT vs DKO cells (**k**) by RT-qPCR. Cells infected with HAV or RV-A2 were harvested after 48h, with EV-71 after 24h and with EMCV after 8h.

For all RT-qPCR experiments, viral RNA was normalized to 18S RNA and results are displayed relative to infection in WT cells. Datasets represent means ± s.e.m. (n=3 biological replicates). P values were determined by unpaired t-test using GraphPad Prism. *, $p<0.05$; **, $p<0.01$; ****<0.0001.

Figure 2

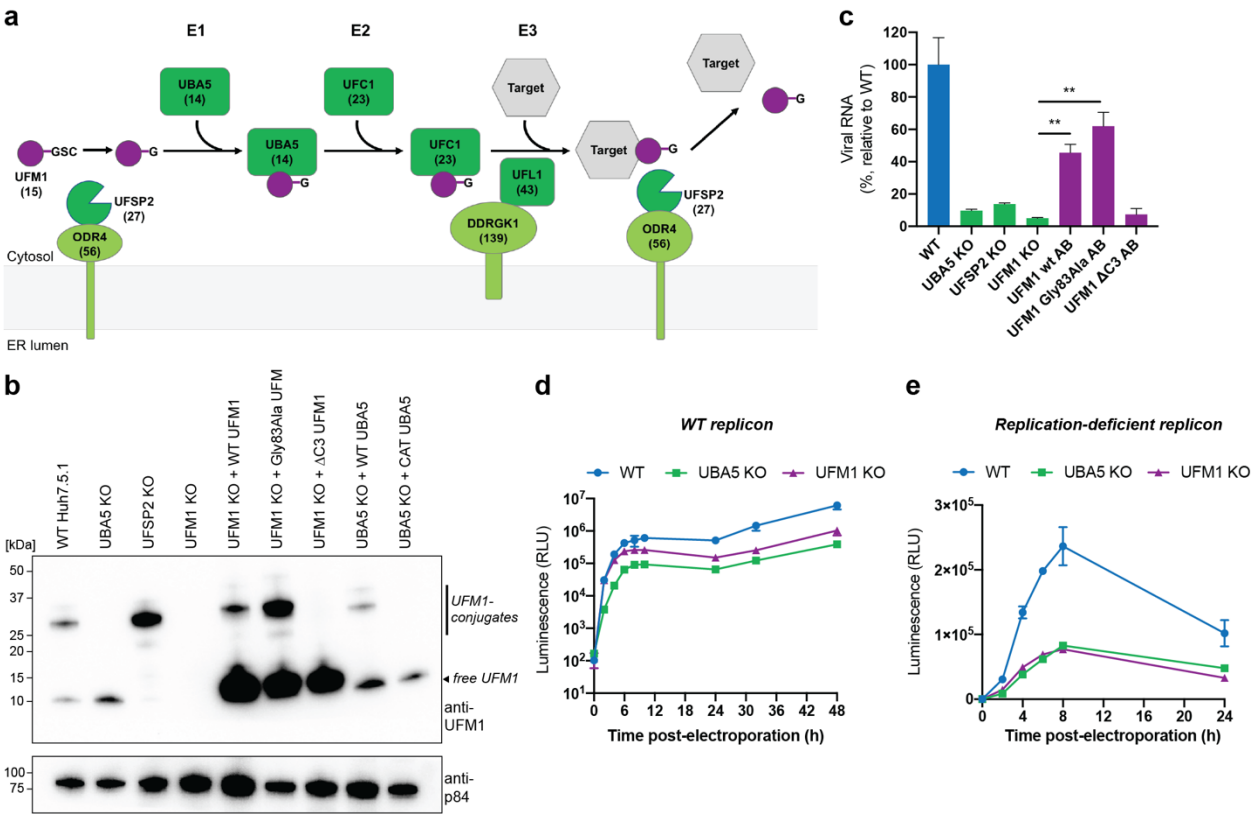

Fig. 2: HAV depends on functional UFM1 conjugation for optimal translation. a, Schematic of cellular UFMylation pathway. (#) indicates rank of gene in the RIGER analysis of CRISPR screen. **b,** UFM1 immunoblot of WT, *UFSP2* KO, *UBA5* KO, *UFM1* KO and *UFM1* KO cells complemented with WT, Gly83Ala or ΔC3 UFM1 as well as *UBA5* KO cells complemented with WT or catalytically inactive UBA5. Upper bands represent UFM1 conjugation products and bottom band represents free UFM1. P84 was used as loading control. **c,** Quantification of HAV RNA in WT, *UFSP2* KO, *UBA5* KO, *UFM1* KO and *UFM1* KO cells complemented with WT, Gly83Ala or ΔC3 UFM1. Viral RNA was normalized to 18S RNA and results are displayed relative to infection in WT cells. Datasets represent means ± s.e.m. (n=3 biological replicates). P values were determined by unpaired t-test using GraphPad Prism. **, p<0.01. **d,** Timecourse of luciferase activity expressed by electroporated HAV-FLuc subgenomic replicon RNA in WT, *UBA5* KO and *UFM1* KO cells. Datasets represent means ± s.d. (n=2 biological replicates) for each timepoint. **e,** Timecourse of luciferase activity expressed by electroporated HAV-FLuc replication-incompetent replicon RNA in WT, *UBA5* KO and *UFM1* KO cells. Datasets represent means ± s.d. (n=2 biological replicates) for each timepoint.

Figure 3

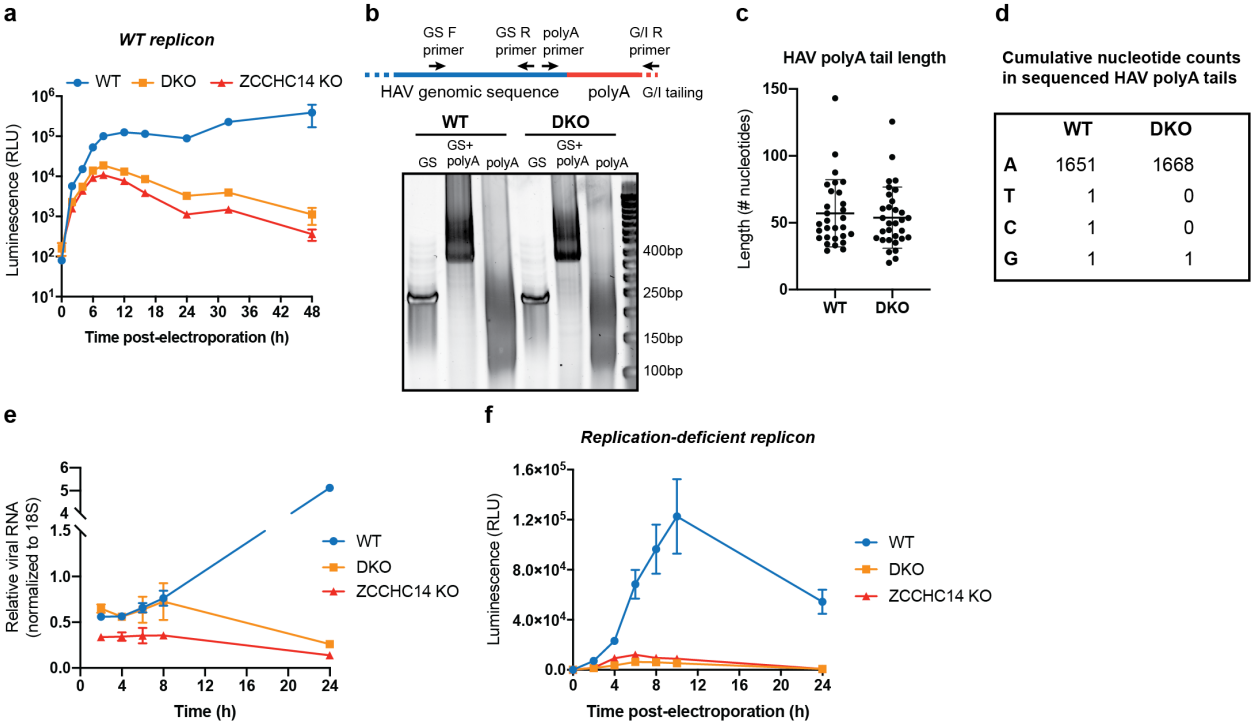

	WT	DKO
A	1651	1668
T	1	0
C	1	0
G	1	1

Fig. 3: TRAMP-like complex is important for viral translation independent of poly(A) tail extension or stabilization. a, Timecourse of luciferase activity expressed by electroporated HAV-FLuc subgenomic replicon RNA in WT, DKO and *ZCCHC14* KO cells. Datasets represent means ± s.d. (n=2 biological replicates) for each timepoint. **b,** HAV poly(A) tail length assay. Total RNA from infected WT or DKO cells was G/I tailed at 3'ends, reverse transcribed and PCR amplified by i) HAV genome-specific (GS) forward and GS reverse primer, ii) GS forward and G/I reverse primer and iii) forward primer upstream of HAV poly(A) start site and G/I reverse primer. PCR products were analyzed by polyacrylamide gel electrophoresis. **c,** Length distribution of sequenced HAV poly(A) tails. An RNA linker was ligated to 3'ends of rRNA-depleted RNA from infected WT or DKO cells followed by reverse transcription and PCR amplification of the HAV poly(A) tail region. PCR products were TOPO cloned and Sanger sequenced. **d,** Analysis of nucleotide composition of sequenced HAV poly(A) tails from (d). **e,** Quantification of HAV RNA in WT, DKO and *ZCCHC14* KO cells by RT-qPCR after cells were infected on ice and incubated at 37C for 1h. Subsequently cells were washed 3 times and bound virus stripped away by trypsinization to prevent any further viral uptake. Finally, cells were harvested at indicated times. Viral RNA was normalized to 18S RNA. Datasets represent means ± s.e.m. (n=3 biological replicates). **f,** Timecourse of luciferase activity expressed by electroporated HAV-FLuc replication-incompetent replicon RNA in WT, DKO cells and *ZCCHC14* KO. Datasets represent means ± s.d. (n=2 biological replicates) for each timepoint.

Figure 4

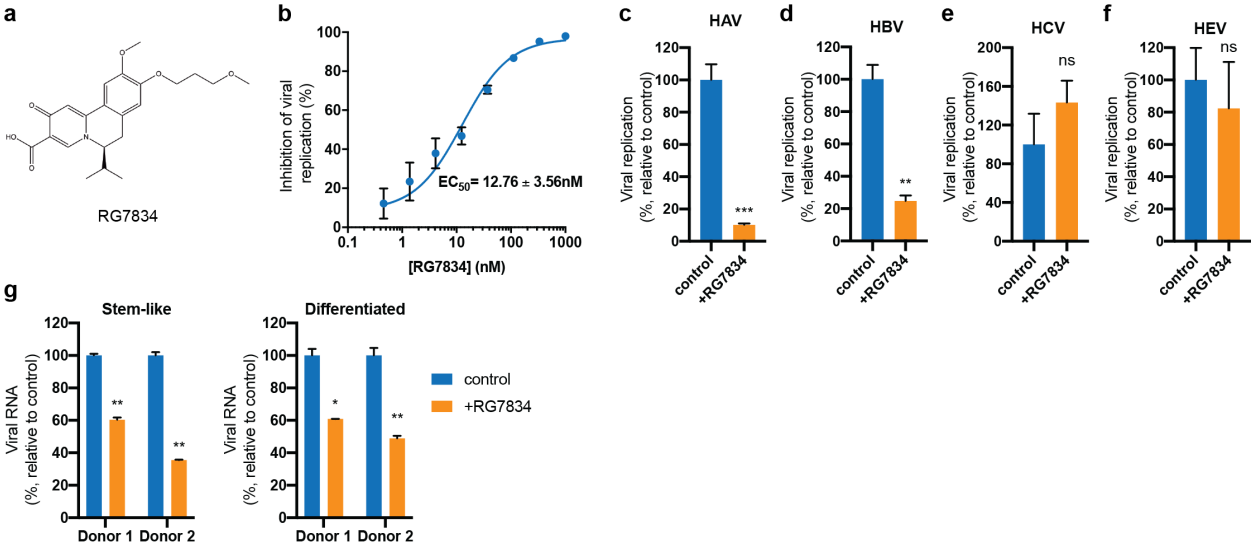

Fig. 4: Small molecule inhibition of PAPD5 and PAPD7 reduces HAV infection in human hepatocyte cells and human liver organoids. a, Chemical structure of RG7834. **b,** Dose-response curve of HAV RNA levels in Huh7.5.1 cells treated with different RG7834 concentrations as measured by RT-qPCR 3 days post-infection/treatment. Non-linear curve was fitted with least squares regression using GraphPad Prism and EC_{50} was determined. **c,** Quantification of HAV RNA in control and RG7834 (100 nM) treated Huh7.5.1 cells 3 dpi by RT-qPCR. **d,** Quantification of HBV total RNA in control and RG7834 (100 nM) treated HepG2-NTCP cells 15 dpi by RT-qPCR. Drug was replenished every 3-4 days. **e,** Quantification of HCV RNA in control and RG7834 (100 nM) treated Huh7.5.1 cells 3 dpi by RT-qPCR. **f,** Quantification of HEV RNA in control and RG7834 (100 nM) treated Huh7.5.1 cells by RT-qPCR 6 days post-transfection of viral RNA. **g,** Quantification of HAV RNA in control and RG7834 (100 nM) treated human liver organoids 7 dpi by RT-qPCR. Organoids were either stem-like or differentiated to adult hepatocytes prior to infection.

For all RT-qPCR experiments, viral RNA was normalized to 18S RNA and results are displayed relative to infection in control (DMSO) condition. Datasets in (**b-f**) represent means ± s.e.m. (n=3 biological replicates). For organoid experiments (**g**) donor 1 and 2 represent 2 independent biological replicates and qPCR was performed with 3 technical replicates. P values were determined by unpaired t-test using GraphPad Prism. ns, non-significant; *, $p<0.05$; **, $p<0.01$; ***, $p<0.001$.

Supplementary Figure1

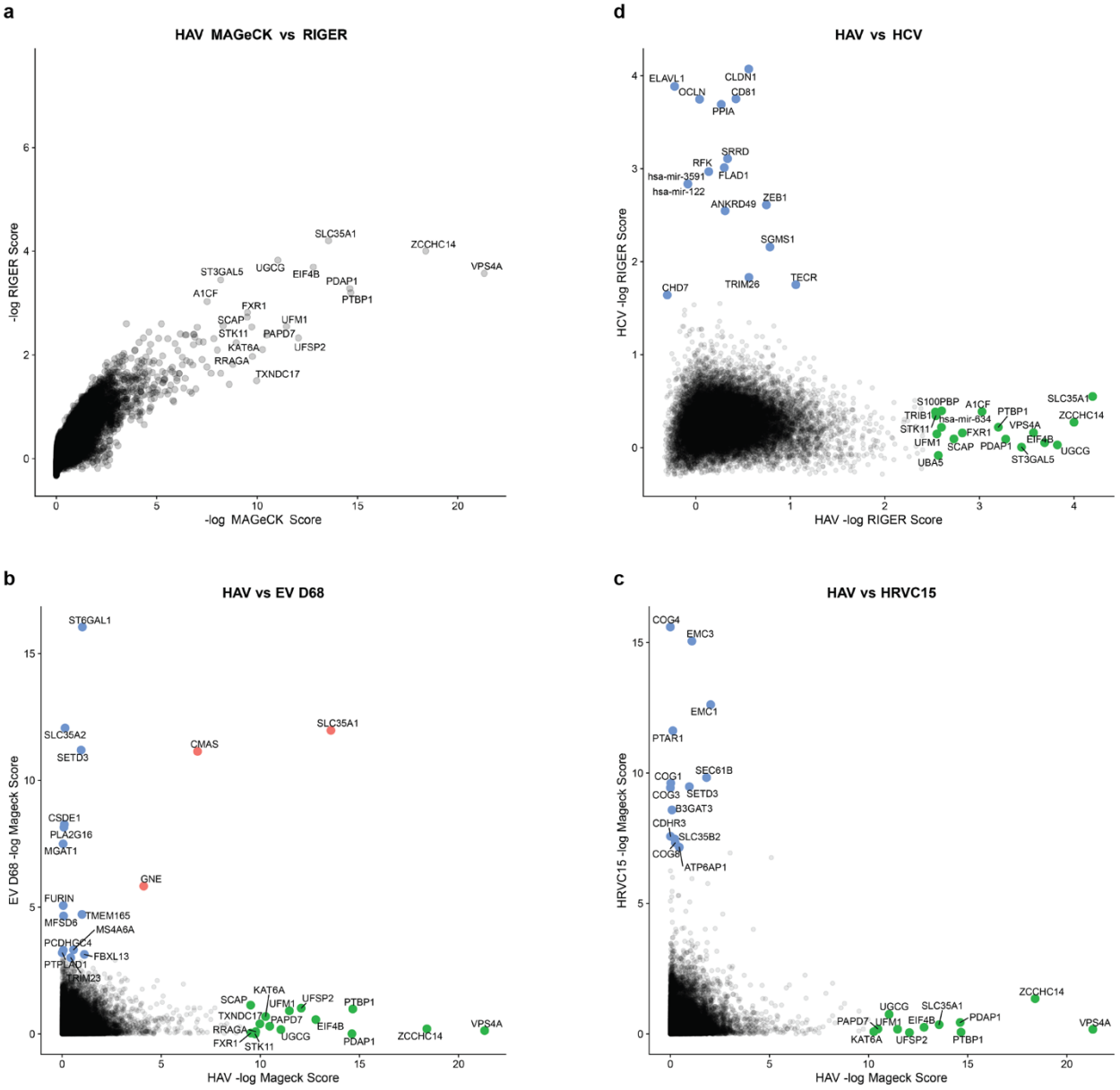

Supplementary Fig. 1: Comparative analysis of CRISPR screen results for HAV, enterovirus D68, rhinovirus C15 and HCV host factors. a, Comparison of RIGER and MaGECK analysis of HAV CRISPR screen. **b,** Comparison of HAV CRISPR screen results from this study with enterovirus D68 CRISPR screen results from [21] using MaGECK analysis. **c,** Comparison of HAV CRISPR screen results from this study with human rhinovirus C15 CRISPR screen results from [21] using MaGECK analysis. **d,** Comparison of HAV CRISPR screen results from this study with HCV CRISPR screen results from [22] using RIGER analysis.

Supplementary Figure 2

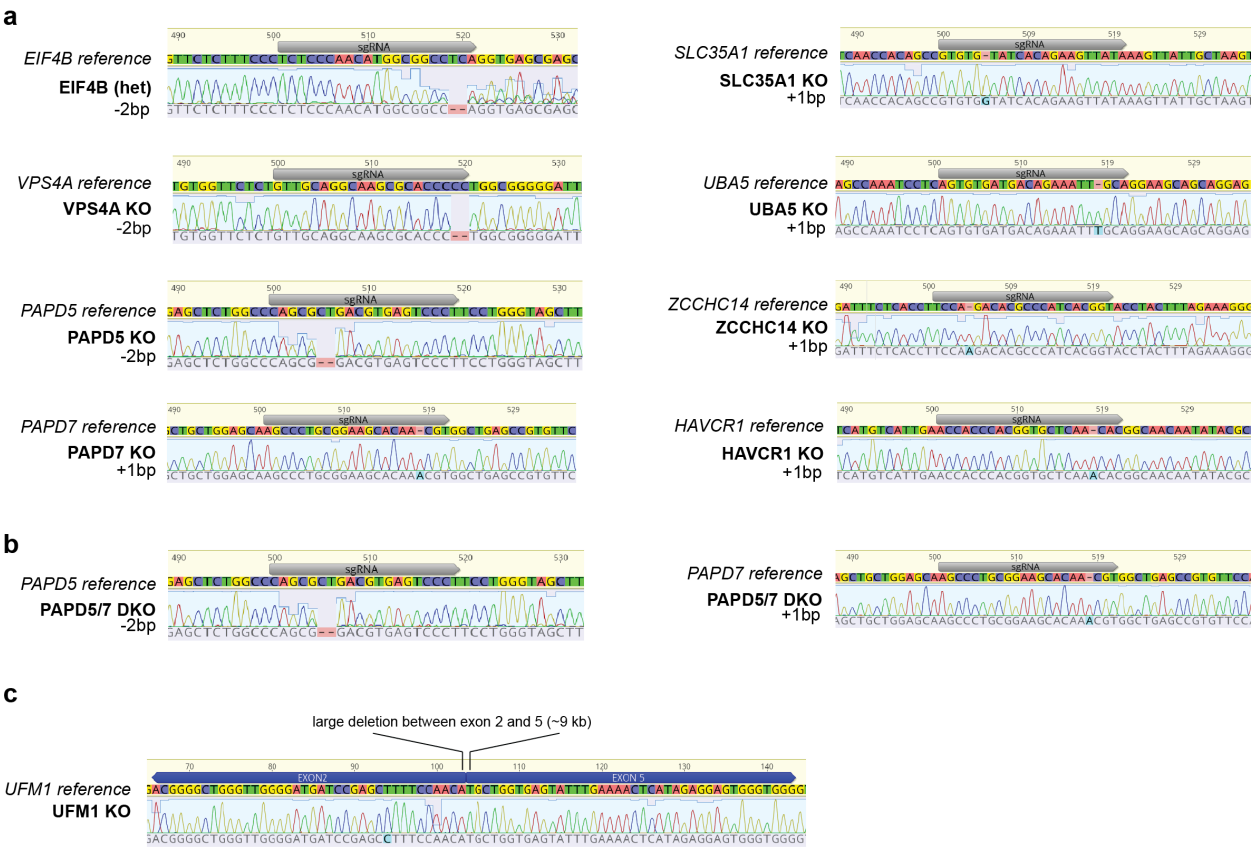

Supplementary Fig. 2: Genotyping of clonal Huh7.5.1 KO cell lines. a, Sanger sequencing of gRNA targeted loci of clonal KO cell lines. Traces were aligned to corresponding reference sequences and indel mutations determined. **b,** Sanger sequencing of gRNA targeted PAPD5 and PAPD7 loci in clonal Huh7.5.1 DKO cells. **c,** Sanger sequencing of UFM1 locus in clonal KO cell line. UFM1 gene was simultaneously targeted by two gRNAs cutting in exon 2 and exon 5 resulting in a large genomic deletion.

Supplementary Figure 3

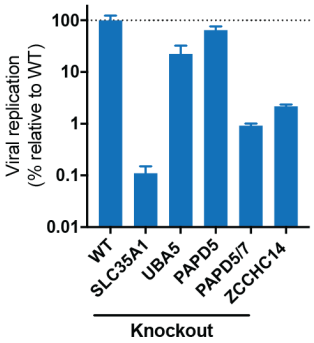

Supplementary Fig. 3: Validation of HAV host factors using a low-passage HAV HM175 strain. Quantification of HAV RNA in WT, or clonal KO cell lines 3 dpi by RT-qPCR. Dotted line indicates 100% infection levels in WT cells. Viral RNA was normalized to 18S RNA and results are displayed relative to infection in WT cells. Datasets represent means ± s.e.m. (n=3 biological replicates).

Supplementary Figure 4

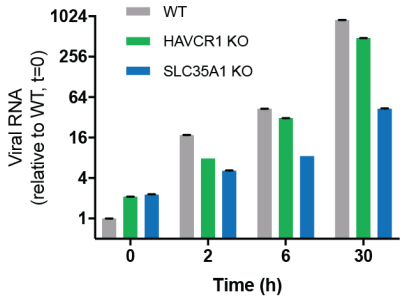

Supplementary Fig. 4: Viral attachment and entry assay. Quantification of HAV RNA in WT, *HAVCR1* KO and *SLC35A1* KO cells by RT-qPCR after cells were infected on ice, washed and incubated at 37C for indicated times. Viral RNA was normalized to 18S RNA and results are displayed relative to infection in WT cells. Datasets represent means ± s.e.m. (n=3 biological replicates).

Supplementary Figure 5

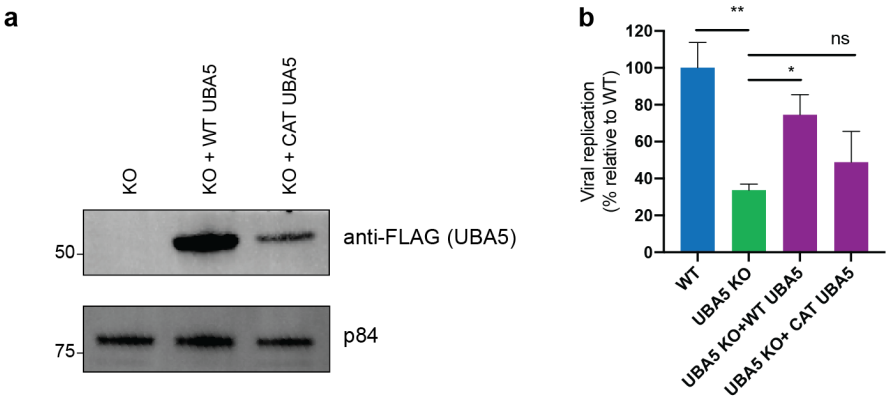

Supplementary Fig. 5: Catalytic activity of UBA5 is required for efficient HAV infection. a, Anti-Anti-FLAG immunoblot of lysates from *UBA5* KO cells transduced with FLAG-tagged WT or catalytically inactive (CAT) UBA5. P84 was used as loading control. **b,** Quantification of HAV RNA in WT, *UBA5* KO and *UBA5* KO complemented with WT or CAT UBA5 3 dpi by RT-qPCR. Viral RNA was normalized to 18S RNA and results are displayed relative to infection in WT cells. Datasets represent means ± s.e.m. (n=3 biological replicates).

Supplementary Figure 6

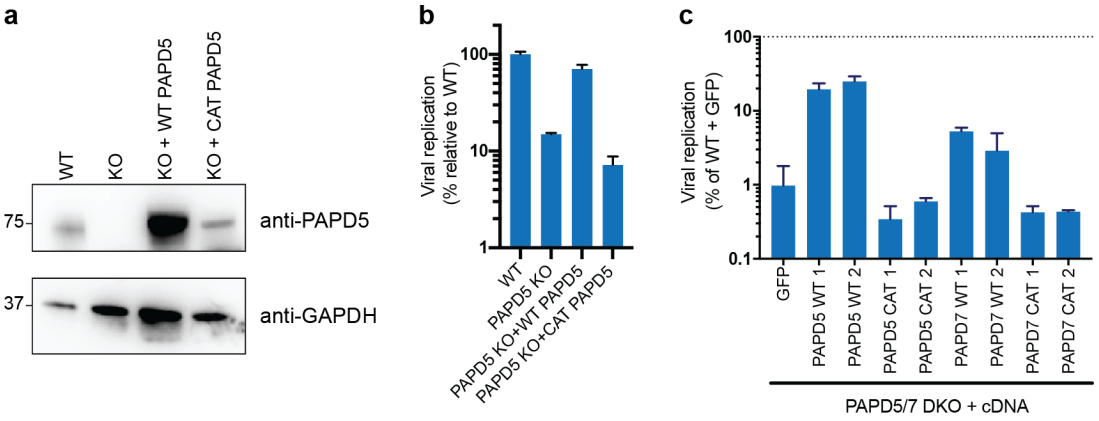

Supplementary Fig. 6: Catalytic activities of PAPD5 and PAPD7 are required for HAV infection. **a,** Anti-PAPD5 immunoblot of lysates from WT, *PAPD5* KO and *PAPD5* KO cells transduced with WT or catalytically inactive (CAT) PAPD5. GAPDH was used as loading control. **b,** Quantification of HAV RNA in WT, *PAPD5* KO and *PAPD5* KO cells complemented with either WT or CAT PAPD5 3 dpi by RT-qPCR. Viral RNA was normalized to 18S RNA and results are displayed relative to infection in WT cells. Datasets represent means ± s.e.m. (n=3 biological replicates). **c,** Quantification of HAV RNA in DKO cells transfected with GFP cDNA, PAPD5 WT or CAT cDNA or PAPD7 WT or CAT cDNA 3 dpi by RT-qPCR. Viral RNA was normalized to 18S RNA and results are displayed relative to infection in WT cells transfected with GFP cDNA. Datasets represent means ± s.e.m. (n=2 biological replicates).

Supplementary Figure 7

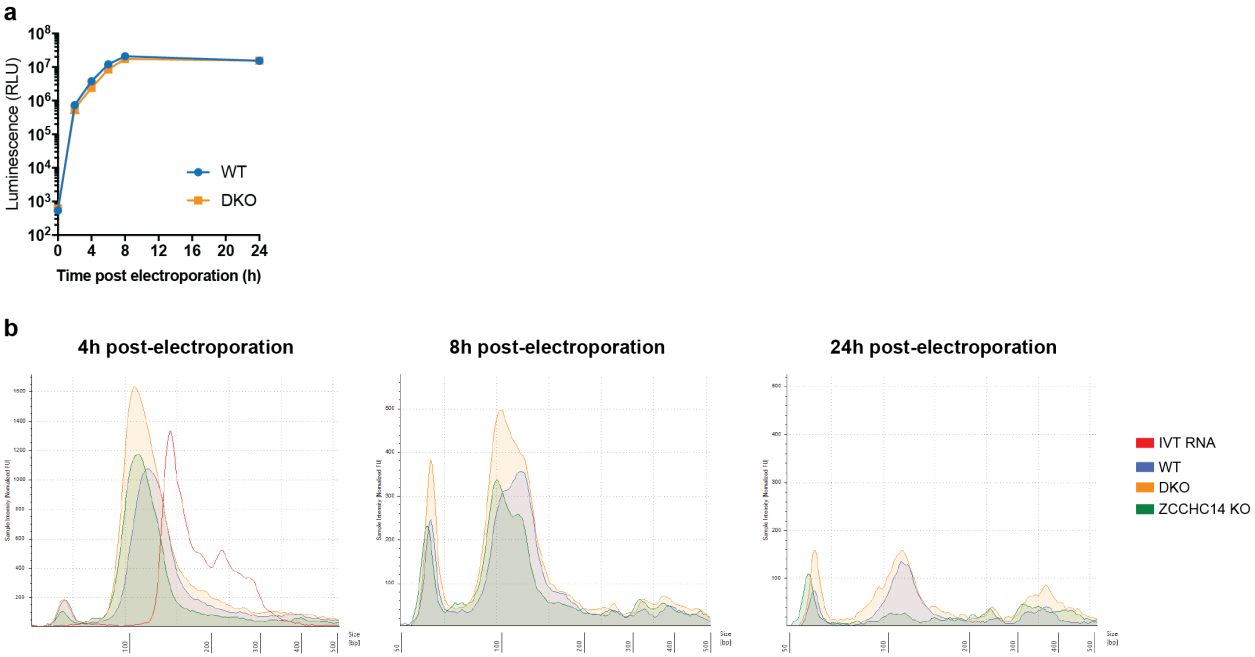

Supplementary Fig. 7: TRAMP-like complex supports viral translation independent of viral RNA stabilization. a, Timecourse of luciferase activity expressed by electroporated firefly mRNA in WT and DKO cells. Datasets represent the means ± s.d. (n=2 biological replicates). **b,** Electrophoretic analysis of poly(A) tail region of electroporated HAV replicon RNA in WT, DKO or *ZCCHC14* KO cells at 4, 8 or 24h post-electroporation. Total RNA from electroporated cells was G/I tailed at 3'ends, reverse transcribed and PCR amplified by forward primer upstream of HAV poly(A) start site and G/I reverse primer. *In-vitro* transcribed (IVT) input RNA was also processed as size reference with expected product size of 124bp.

Supplementary Figure 8

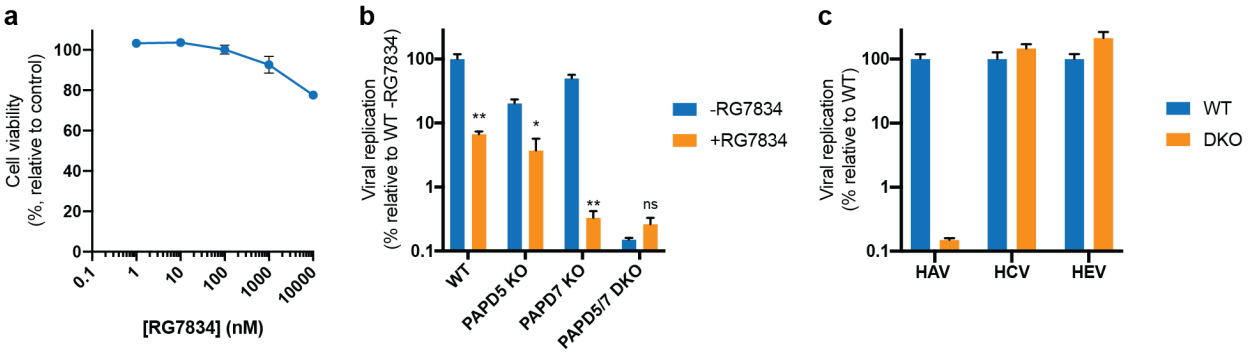

Supplementary Fig. 8: Characterization of RG7834 in Huh7.5.1 cells and comparison of PAPD5/7 dependency among hepatitis viruses. a, Cell viability assay of Huh7.5.1 cells treated with different concentrations of RG7834 for 3 days. Dataset represents means ± s.d. (n=3 biological replicates) for each time point and values are relative to DMSO treated control. **b,** Quantification of HAV RNA in WT, *PAPD5* KO, *PAPD7* KO or DKO cells untreated or treated with 100 nM RG7834 3 dpi by RT-qPCR. **c,** Quantification of HAV, HCV or HEV RNA in WT or DKO cells 3 or 5 dpi by RT-qPCR.

For RT-qPCR experiments, viral RNA was normalized to 18S RNA and results are displayed relative to infection in (untreated) WT cells. Datasets represent means ± s.e.m. (n=3 biological replicates).

Methods

Cell lines, viruses and reagents

Huh7.5.1 (gift from Frank Chisari) and HEK293FT (Thermo Scientific) were cultured in DMEM (Gibco) supplemented with 10% fetal bovine serum (FBS, Omega Scientific), penicillin/streptomycin (Gibco), non-essential amino acids (Gibco) and L-glutamine (Gibco) at 37C and 5% CO_2. HepG2-NTCP-K7 cells[53] (gift from Ulrike Protzer) and HepAD38 cells[54] (gift from Christoph Seeger) were cultured in DMEM/F12 (Gibco) supplemented with 10% FBS, penicillin/streptomycin, non-essential amino acids, L-glutamine and sodium pyruvate (Gibco) at 37C and 5% CO_2. Cell lines were tested negative for mycoplasma and were authenticated by STR profiling. Hepatitis A virus HM175/18f (NR-137) was obtained through BEI Resources (NIAID, NIH) and HM175/clone 1 (VR-1541) through ATCC. HAV strains were propagated in Huh7.5.1 cells grown in adeno expression media (Gibco) supplemented with penicillin/streptomycin, non-essential amino acids and L-glutamine, supernatant was collected 5-12 dpi and filtered (0.45 micron). To generate concentrated HAV stocks, supernatant was incubated with 8% PEG-8000 at 4C overnight, centrifuged at 3,200g for 60min and pellet was resuspended in a small volume of DMEM with 10% FBS and aliquoted. For the generation of HAV-Nluc (gift from Stanley Lemon)[55], the infectious clone plasmid was linearized, RNA was *in-vitro* transcribed using MEGAscript T7 Transcription Kit (Invitrogen) and transfected into Huh7.5.1 cells using TransIT-LT1 Transfection Reagent (Mirus Bio). Subsequently, cell supernatant was collected 8-13dpi, filtered and aliquoted. Purified encephalomyocarditis virus (NR-46441) was obtained through BEI Resources (NIAID, NIH). Enterovirus 71 (MP4), rhinovirus A2 and HCV JFH1 stocks were kindly provided by Jan Carette. For HBV production, supernatant was collected from HepAD38 cells, filtered (0.45 micron), and concentrated using 8% PEG-8000 as described above. The HEV infectious clone (genotype 3) was obtained from the NIH/NIAID and viral RNA was generated by *in-vitro* transcription from linearized plasmid[56]. For virus stocks, titers were determined by plaque- or focus-forming assay. RG7834 was purchased from MedKoo Biosciences and resuspended in DMSO at 50mg/ml. Puromycin and blasticidin were obtained from Gibco.

CRISPR host factor screen

Huh7.5.1 cells were stably transduced with lentivirus from lentiCas9-Blast (Addgene #52962, gift from Feng Zhang) and subsequently selected using blasticidin. Next, a total of 300 million Huh7.5.1-Cas9 cells were then transduced with lentivirus containing the human GeCKO v2 library (Addgene #1000000049, gift from Feng Zhang) at a multiplicity of infection (MOI) of 0.3, subsequently selected using puromycin and expanded for 10 days. A total of 60 million mutagenized cells for each sublibrary (A and B) were collected for genomic DNA extraction, and a total of 45 million mutagenized cells for each sublibrary were infected with 15ml of unconcentrated HAV HM175/18f per T175 flask (1:1 diluted with fresh DMEM media). An additional 15ml of media was added after 2h. Media was refreshed 4 and 8dpi and surviving cells

were collected 12dpi for genomic DNA extraction using QIAamp DNA Blood Maxi Kit (Qiagen). gRNA encoding DNA sequences were amplified in a two-step nested PCR using KAPA HiFi HotStart ReadyMixPCR Kit (Kapa Biosystems) and sequenced on an Illumina NextSeq (High Output) (for primer sequences, see Supplementary Table 4). For analysis, reads were aligned to gRNA reference table, enrichment of each gRNA was calculated by comparing the relative abundance in the selected and unselected cell population and gene significance was calculated using RIGER (using weighted sum) or MaGeCK[57,58]. Gene ontology analysis of enriched genes in target list (RIGER p-value < 0.001) was performed using GOrilla[59].

Generation of clonal KO cell lines

Oligos containing gRNA sequence were annealed and ligated into pX458 (Addgene #48138, gift from Feng Zhang). Cells were transfected with pX458 constructs using Lipofectamine 3000 (Invitrogen) and two days later GFP positive cells were single-cell sorted into 96-well plates using a Sony SH800 cell sorter. For genotyping, genomic DNA was isolated from obtained clones using QuickExtract (Lucigen), the gRNA-targeted sites PCR amplified and the products Sanger-sequenced. Obtained sequences were compared to reference sequences for indel mutations or large deletion. A list of all used sgRNA oligo and genotyping primer sequences can be found in Supplementary Table 4.

RT-qPCR assays

Cells were plated in 96-well plates (in triplicates for each condition) and infected the next day with virus at the following MOIs: HAV (~5-50 FFU/cell), RV-A2 (~1 PFU/cell), EV-71 (~0.2 PFU/cell), EMCV (~0.2 PFU/cell), HCV (~1 FFU/cell) and HBV (~1 FFU/cell). Cells were harvested, lysates reverse transcribed and quantitative PCR performed on a Bio-Rad CFX96 Touch system using the Power SYBR Cells-to-CT kit (Invitrogen). All viral RNA levels were normalized to 18S levels. Primer sequences can be found in Supplementary Table 4.

Viral attachment and entry assay

96-well plates containing WT, *SLC35A1* KO or *HAVCR1* KO Huh7.5.1 cells were chilled on ice before infection with HAV HM175/18f at an MOI of 500 FFU/cell. Cells were incubated for 1h on ice before moving them to a 37C incubator. At each harvest timepoint, cells were washed three times with PBS and processed for RT-qPCR as described above.

HAV nanoluciferase reporter assay

Cells were plated in 96-well plates and infected the next day with equal amounts of HAV-Nluc. Lysates were harvested by washing once with PBS wash followed by addition of 22µl of Passive Lysis Buffer (Promega) under shaking for 15min. For luminescence readout, 15µl of lysate were mixed with 50µl of Nano-Glo assay buffer (Promega) in a flat bottom white-walled luminescence

plate, incubated for 5min at room temperature and read on an EnVision plate reader (PerkinElmer).

Complementation of KO cells with cDNA

UBA5 cDNA was obtained from Dharmacon (DNA Accession: BC009737, Clone ID: 3879061). To generate cDNA encoding catalytically inactive enzyme, a Cys250Arg mutation was introduced by PCR. Additionally, a C-terminal FLAG-tag was added to WT and CAT cDNA sequences. UFM1 was obtained from Dharmacon (cDNA Accession: BC005193, Clone ID: 3829206). N-terminal FLAG and C-terminal mutations (Gly83Ala or ΔC3 (deletion of GlySerCys)) were introduced by PCR. ZCCHC14 cDNA was obtained from Dharmacon (cDNA Accession: BC101478, Clone ID: 8068984). The N-terminus was extended using a Gblock (Integrated DNA Technologies) resembling the protein coding sequence for a longer isoform (1086 amino acids, ENST00000671377.1) to match the molecular weight of ZCCHC14 detected in WT Huh7.5.1 by immunoblot. PCR products were gel-purified and cloned into into EcoRV-cut pLenti CMV Puro DEST (w118-1) (Addgene #17452, gift from Eric Campeau & Paul Kaufman) using NEBuilder HiFi DNA Assembly Master Mix (New England BioLabs). Lentivirus was produced in HEK293FT and collected 48h post-transfection. KO cells were transduced with filtered, lentiviral containing supernatant under addition of polybrene and selected using 4 µg/ml puromycin for 3-4 days. For PAPD5 and PAPD7, pCI3 plasmids with WT or catalytic mutant cDNA sequences were kindly provided by V. Narry Kim and were described previously[36]. For transient complementation, plasmids were transfected into WT or DKO cells using TransIT-LT1 Transfection Reagent (Mirus Bio), and transfected cells were plated in 96-wells the next day for HAV infection. To generate stable cell lines, cDNA sequences were cloned into the PB-CMV-MCS-EF1α-Puro vector (PB510B-1, SBI System Biosciences) where the CMV promoter was replaced by a PGK promoter. Plasmids were co-transfected together with a plasmid expressing piggyBac transposase into *PAPD5* KO cells, which were subsequently selected with puromycin for 5 days starting 3 days post-transfection. All primer sequences can be found in Supplementary Table 4.

Immunoblotting

Cell were lysed using Laemmli SDS sample buffer containing 5% beta-mercaptoethanol and boiled for 10min. Lysates were separated by SDS-PAGE on pre-cast Bio-Rad 4-15% poly-acrylamide gels in Bio-Rad Mini-Protean electrophoresis system. Proteins were transferred onto PVDF membranes using Bio-Rad Trans-Blot Turbo transfer system. PVDF membranes were blocked with PBS buffer containing 0.1% Tween-20 and 5% non-fat milk. Blocked membranes were incubated with primary antibody diluted in blocking buffer and incubated overnight at 4C on a shaker. Primary antibodies were detected by incubating membranes with 1:4000 dilution of HRP-conjugated (Southern Biotech) or 1:5000 dilution of IRDye-conjugated (LI-COR) secondary anti-mouse and anti-rabbit antibodies for 1 h at room temperature. Blots were visualized using a

ChemiDoc MP Imaging System (Bio-Rad). The following primary antibodies (and their dilutions) were used in this study: p84 (Genetex, GTX70220) at 1:1000, GAPDH (SCBT, sc-32233) at 1:1000, FLAG M2 (Sigma, F1804) at 1:1000, UFM1 (Abcam, ab109305) at 1:1000, PAPD5 (Atlas Antibodies, HPA042968) at 1:1000 and ZCCHC14 (Bethyl, A303-096A) at 1:1000.

Replicon assay

The replicon plasmids pLuc-HAV/18f and pLuc-HAV/18f-3D^{pol}GDD→GAA (replication-defective mutant) were kindly provided by Stanley Lemon and were described previously[60]. Plasmids were linearized using MluI-HF (New England BioLabs), RNA was generated using the MEGAscript T7 Kit (Invitrogen) and subsequently purified by lithium chloride precipitation. For electroporation, 1-2 million cells were washed three times in PBS, resuspended in 100µl SF Nucleofector solution (Lonza), mixed with 250ng replicon RNA per 80k cells, transferred to a 100 µl nucleocuvette and pulsed using the program FF-137 on an Amaxa 4D-Nucleofector X Unit (Lonza). Cells were then resuspended in equilibrated, antibiotic-free medium, distributed into 96-wells and lysed at different timepoints post-electroporation using 40µl Passive Lysis buffer (Promega). Luminescence was measured using Luciferase Assay System (Promega) on a white-walled luminescence plate with an EnVision plate reader (PerkinElmer).

Poly(A) tail length assay by polyacrylamide gel electrophoresis

Cells were infected with HAV HM175/18f (MOI=10) and harvested 3 days post-infection using Trizol (Invitrogen). RNA was purified with Direct-zol RNA Microprep columns (Zymo Research). HAV poly(A) tails were analyzed using the Poly(A) Tail-Length Assay Kit (Thermo Scientific) according to the manufacturer's instructions. Briefly, 1µg total RNA per condition was used as input for G/I tailing reaction followed by reverse transcription. Next, RT products were amplified using different PCR primer combinations: i) HAV genome-specific (GS) forward and GS reverse primer, ii) GS forward and G/I reverse primer and iii) forward primer upstream of HAV poly(A) start site and G/I reverse primer. Finally, PCR products were analyzed using polyacrylamide gel electrophoresis on a 5% Mini-PROTEAN Tris/Boric Acid/EDTA (TBE) gel in TBE buffer (100V for 60min). Gel was stained with SYBR Gold (diluted 1:10000 in TBE buffer) for ~30min in the dark and imaged on a ChemiDoc MP Imaging System (Bio-Rad).

Poly(A) tail sequencing

RNA was isolated from infected cells as described above. Ribosomal RNA (rRNA) was depleted from 1µg total RNA by addition of rRNA Removal Mix – Gold (Illumina) followed by incubation at 68C for 5min, addition of rRNA Removal Beads (Illumina), removal of supernatant while tubes are on a magnetic rack, and finally elution of rRNA-depleted RNA. Next, a 5´ adenylated, 3´ blocked oligodeoxynucleotide RNA linker (S1315S, New England BioLabs) was ligated to the 3' ends of RNAs by incubation with RNA ligase 2, truncated (New England BioLabs) for 3h at 22C.

Ligation products were then reverse transcribed using a primer, which is reverse complement to the RNA linker, and Superscript IV (Invitrogen). Finally, HAV poly(A) tails were specifically amplified in a nested PCR, cloned into the pCRBlunt II-TOPO vector (Invitrogen) and Sanger sequenced (Quintarabio). Number of adenosines downstream of the HAV 3'UTR region and occurrence of non-adenosine nucleotides were counted.

Tapestation analysis of poly(A) tails of replicon RNA

10^6 cells were electroporated with *in-vitro* transcribed replicon RNA containing a 40bp long poly(A) tail as described above. For each timepoint, cells were washed with PBS, trypsined, pelleted and lysed using Trizol followed by RNA extraction with Direct-zol columns. Total RNA was G/I tailed, reverse transcribed and poly(A) tail region was amplified using forward primer upstream of HAV poly(A) start site and G/I reverse primer. Additionally, *in-vitro* transcribed replicon RNA was directly processed. Products were analyzed using a High Sensitivity D1000 ScreenTape System (Agilent).

Cell viability assay

Huh7.5.1 cells were treated with different concentrations of RG7834 for 3 days and viability was measured using Cell Titer Glo (Promega) according to the manufacturer's instructions.

Culture and HAV infection of human liver organoids

Bi-potent stem cell organoids were generated as previously described[39,61]. Briefly, we obtained liver tissue samples from the healthy resection margins of partial hepatectomies. Following tissue digest, the heterogeneous mixture of single cells was suspended in reduced growth factor BME2 (Basement Membrane Extract, Type 2, Trevigen). From this mixture, 50 µL drops containing 1,000 to 20,000 cells were seeded in 24-well suspension culture plates (GreinerBio). Drops were incubated at 37C for >20 min and solidified. After this, 500 µL of expansion media (EM) was added to each well. Expansion media is basal media (Advanced DMEM/F12 with 1% penicillin/streptomycin, 1% Glutamax, and 10 mM HEPES (all from ThermoFisher)) supplemented with 1% N2 (Gibco), 1% B27 (Gibco), 1 mM N-Acetylcysteine (Sigma-Aldrich), 10 nM [Leu^{15}]-gastrin I human (Sigma-Aldrich), 10% (vol/vol) R-spondin1 conditioned media (generated as described in [39]), and 10 mM Nicotinamide (Sigma-Aldrich). Expansion media additionally contains 50 ng/ml recombinant human EGF, 25 ng/ml recombinant human HGF, 100 ng/ml recombinant human FGF10, 10 µM Forskolin, and 5 µM A83-01 (all from Stem Cell Technologies). Expansion media was replaced every 3-4 days. Organoids in expansion media grew in culture for 4-6 months and needed to be routinely passaged with TRYPLE (Gibco). To induce differentiation to a hepatocyte-like fate, expansion media was supplemented with 25 ng/ml BMP7 (ProSpec) for 3-4 days. After this, media was changed to differentiation media (DM). Differentiation media is basal media supplemented with 1% N2, 1% B27, 1 mM N-acetylcysteine, 10 nM [Leu^{15}]-gastrin I human,

50 ng/ml EGF, 25 ng/ml HGF, 0.5 µM A83-01, 25 ng/ml BMP7, 3 µM dexamethasone (Sigma-Aldrich), 10 µM DAPT (Stem Cell Technologies), and 100 ng/ml recombinant human FGF19 (ProSpec). Differentiation media was changed every 3-4 days for a period of 3-15 days. For HAV infection, organoid lines from two non-viral donors were spin-infected with the HM175/18f strain of HAV as follows. Organoids from EM and DM d3 conditions were collected and lightly dissociated by a 3 min incubation at 37°C with TRYPLE. Cells were then suspended in basal media containing 10 µM Y-27632 (Stem Cell Technologies) and counted. These cells were mixed with HAV at an MOI of 500 FFU/cell in the presence and absence of RG7834 at 100nM. Cell suspensions were then added to a 24-well suspension culture plate. The plate was centrifuged at 600 x g for 1 h at room temperature, followed by a 2 h incubation at 37C. After this, cells were collected and washed 3x in basal media. Washed cells were seeded in fresh BME2 drops in a new 24-well suspension culture plate. At 7 days post-infection, infected organoid samples were washed 2x in cold basal media, and cell pellets were lysed in Trizol.

Supplementary Tables

Supplementary Table 1: Hepatitis A virus CRISPR screen results.
Supplementary Table 2: Gene ontology analysis of genes enriched in CRISPR screen.
Supplementary Table 3: Sanger sequencing reads of cloned HAV poly(A) tails
Supplementary Table 4: Oligo sequences.

Author contributions

JK and ASP were responsible for design and execution of experiments, data analysis and manuscript preparation. RW performed comparative analysis of CRISPR screens and assisted with molecular biology experiments. NLM conducted organoid experiments under the supervision of MO. ASP conceptualized and supervised the study.

Acknowledgments

We would like to thank Don Ganem for helpful discussions and critically reading the manuscript, the Biohub Genomics platform for help with sequencing, James Webber for assistance with the CRISPR screen analysis, and members of the Biohub Infectious Disease Initiative for helpful discussions. We would like to acknowledge Drs. Stanley Lemon (University of North Carolina, Chapel Hill), Jan Carette (Stanford University), V. Narry Kim (Seoul National University), Ulrike Protzer (Technical University Munich), Feng Zhang (Broad Institute), Christoph Seeger (Fox Chase Cancer Center) and Suzanne Emerson (NIH) for providing critical reagents. We also acknowledge Dr. Stewart Cooper and Ann Erickson who oversee the Ibrahim El-Hefni Liver Biorepository at the California Pacific Medical Center Research Institute and provided patient tissue samples used to generate liver organoids. The research was funded by the Chan Zuckerberg Biohub (ASP) and by NIH/NIDA grants AI097552 and DP1DA038043-01 (MO).

References

1. Jacobsen, K. H. Globalization and the Changing Epidemiology of Hepatitis A Virus. *Cold Spring Harb. Perspect. Med.* **8**, a031716 (2018).
2. CDC. Widespread person-to-person outbreaks of hepatitis A across the United States | CDC. https://www.cdc.gov/hepatitis/outbreaks/2017March-HepatitisA.htm (2019).
3. Drake, M. J. *et al.* A role for glycolipid biosynthesis in severe fever with thrombocytopenia syndrome virus entry. *PLOS Pathog.* **13**, e1006316 (2017).
4. Ding, S. *et al.* STAG2 deficiency induces interferon responses via cGAS-STING pathway and restricts virus infection. *Nat. Commun.* **9**, 1–8 (2018).
5. Baggen, J. *et al.* Enterovirus D68 receptor requirements unveiled by haploid genetics. *Proc. Natl. Acad. Sci.* **113**, 1399–1404 (2016).
6. Han, J. *et al.* Genome-wide CRISPR/Cas9 Screen Identifies Host Factors Essential for Influenza Virus Replication. *Cell Rep.* **23**, 596–607 (2018).
7. Avanzino, B. C., Fuchs, G. & Fraser, C. S. Cellular cap-binding protein, eIF4E, promotes picornavirus genome restructuring and translation. *Proc. Natl. Acad. Sci.* **114**, 9611–9616 (2017).
8. Borman, A. M., Michel, Y. M. & Kean, K. M. Detailed Analysis of the Requirements of Hepatitis A Virus Internal Ribosome Entry Segment for the Eukaryotic Initiation Factor Complex eIF4F. *J. Virol.* **75**, 7864–7871 (2001).
9. Pestova, T. V., Hellen, C. U. & Shatsky, I. N. Canonical eukaryotic initiation factors determine initiation of translation by internal ribosomal entry. *Mol. Cell. Biol.* **16**, 6859–6869 (1996).
10. Kafasla, P., Lin, H., Curry, S. & Jackson, R. J. Activation of picornaviral IRESs by PTB shows differential dependence on each PTB RNA-binding domain. *RNA N. Y. N* **17**, 1120–1131 (2011).
11. Votteler, J. & Sundquist, W. I. Virus Budding and the ESCRT Pathway. *Cell Host Microbe* **14**, 232–241 (2013).
12. Feng, Z. *et al.* A pathogenic picornavirus acquires an envelope by hijacking cellular membranes. *Nature* **496**, 367–371 (2013).
13. Komatsu, M. *et al.* A novel protein-conjugating system for Ufm1, a ubiquitin-fold modifier. *EMBO J.* **23**, 1977–1986 (2004).
14. Lubas, M. *et al.* Interaction Profiling Identifies the Human Nuclear Exosome Targeting Complex. *Mol. Cell* **43**, 624–637 (2011).
15. McKnight, K. L. & Lemon, S. M. Hepatitis A Virus Genome Organization and Replication Strategy. *Cold Spring Harb. Perspect. Med.* a033480 (2018) doi:10.1101/cshperspect.a033480.
16. Puschnik, A. S., Majzoub, K., Ooi, Y. S. & Carette, J. E. A CRISPR toolbox to study virus–host interactions. *Nat. Rev. Microbiol.* **15**, 351–364 (2017).

17. Gerakis, Y., Quintero, M., Li, H. & Hetz, C. The UFMylation System in Proteostasis and Beyond. *Trends Cell Biol.* **29**, 974–986 (2019).
18. Warkocki, Z., Liudkovska, V., Gewartowska, O., Mroczek, S. & Dziembowski, A. Terminal nucleotidyl transferases (TENTs) in mammalian RNA metabolism. *Philos. Trans. R. Soc. B Biol. Sci.* **373**, 20180162 (2018).
19. Go, C. D. *et al.* A proximity biotinylation map of a human cell. *bioRxiv* 796391 (2019) doi:10.1101/796391.
20. Hamill, S., Wolin, S. L. & Reinisch, K. M. Structure and function of the polymerase core of TRAMP, a RNA surveillance complex. *Proc. Natl. Acad. Sci. U. S. A.* **107**, 15045–15050 (2010).
21. Diep, J. *et al.* Enterovirus pathogenesis requires the host methyltransferase SETD3. *Nat. Microbiol.* (2019) doi:10.1038/s41564-019-0551-1.
22. Marceau, C. D. *et al.* Genetic dissection of Flaviviridae host factors through genome-scale CRISPR screens. *Nature* **535**, 159–163 (2016).
23. Kaplan, G. *et al.* Identification of a surface glycoprotein on African green monkey kidney cells as a receptor for hepatitis A virus. *EMBO J.* **15**, 4282–4296 (1996).
24. Das, A. *et al.* TIM1 (HAVCR1) Is Not Essential for Cellular Entry of Either Quasi-enveloped or Naked Hepatitis A Virions. *mBio* **8**, (2017).
25. Tatsumi, K. *et al.* A novel type of E3 ligase for the Ufm1 conjugation system. *J. Biol. Chem.* **285**, 5417–5427 (2010).
26. Kang, S. H. *et al.* Two novel ubiquitin-fold modifier 1 (Ufm1)-specific proteases, UfSP1 and UfSP2. *J. Biol. Chem.* **282**, 5256–5262 (2007).
27. Chen, C., Itakura, E., Weber, K. P., Hegde, R. S. & de Bono, M. An ER complex of ODR-4 and ODR-8/Ufm1 specific protease 2 promotes GPCR maturation by a Ufm1-independent mechanism. *PLoS Genet.* **10**, e1004082 (2014).
28. Wu, J., Lei, G., Mei, M., Tang, Y. & Li, H. A novel C53/LZAP-interacting protein regulates stability of C53/LZAP and DDRGK domain-containing Protein 1 (DDRGK1) and modulates NF-kappaB signaling. *J. Biol. Chem.* **285**, 15126–15136 (2010).
29. Rammelt, C., Bilen, B., Zavolan, M. & Keller, W. PAPD5, a noncanonical poly(A) polymerase with an unusual RNA-binding motif. *RNA* **17**, 1737–1746 (2011).
30. Shin, J., Paek, K. Y., Ivshina, M., Stackpole, E. E. & Richter, J. D. Essential role for non-canonical poly(A) polymerase GLD4 in cytoplasmic polyadenylation and carbohydrate metabolism. *Nucleic Acids Res.* **45**, 6793–6804 (2017).
31. Shcherbik, N., Wang, M., Lapik, Y. R., Srivastava, L. & Pestov, D. G. Polyadenylation and degradation of incomplete RNA polymerase I transcripts in mammalian cells. *EMBO Rep.* **11**, 106–111 (2010).
32. Boele, J. *et al.* PAPD5-mediated 3' adenylation and subsequent degradation of miR-21 is disrupted in proliferative disease. *Proc. Natl. Acad. Sci. U. S. A.* **111**, 11467–11472 (2014).

33. Berndt, H. *et al.* Maturation of mammalian H/ACA box snoRNAs: PAPD5-dependent adenylation and PARN-dependent trimming. *RNA* **18**, 958–972 (2012).
34. Vaňáčová, Š. *et al.* A New Yeast Poly(A) Polymerase Complex Involved in RNA Quality Control. *PLOS Biol.* **3**, e189 (2005).
35. Hyrina, A. *et al.* A Genome-wide CRISPR Screen Identifies ZCCHC14 as a Host Factor Required for Hepatitis B Surface Antigen Production. *Cell Rep.* **29**, 2970-2978.e6 (2019).
36. Lim, J. *et al.* Mixed tailing by TENT4A and TENT4B shields mRNA from rapid deadenylation. *Science* **361**, 701–704 (2018).
37. Mueller, H. *et al.* A novel orally available small molecule that inhibits hepatitis B virus expression. *J. Hepatol.* **68**, 412–420 (2018).
38. Mueller, H. *et al.* PAPD5/7 Are Host Factors That Are Required for Hepatitis B Virus RNA Stabilization. *Hepatology* **69**, 1398–1411 (2019).
39. Broutier, L. *et al.* Culture and establishment of self-renewing human and mouse adult liver and pancreas 3D organoids and their genetic manipulation. *Nat. Protoc.* **11**, 1724–1743 (2016).
40. Walczak, C. P. *et al.* Ribosomal protein RPL26 is the principal target of UFMylation. *Proc. Natl. Acad. Sci. U. S. A.* **116**, 1299–1308 (2019).
41. Wang, L. *et al.* UFMylation of RPL26 links translocation-associated quality control to endoplasmic reticulum protein homeostasis. *Cell Res.* (2019) doi:10.1038/s41422-019-0236-6.
42. Majzoub, K. *et al.* RACK1 controls IRES-mediated translation of viruses. *Cell* **159**, 1086–1095 (2014).
43. Landry, D. M., Hertz, M. I. & Thompson, S. R. RPS25 is essential for translation initiation by the Dicistroviridae and hepatitis C viral IRESs. *Genes Dev.* **23**, 2753–2764 (2009).
44. Schmid, M. & Jensen, T. H. Controlling nuclear RNA levels. *Nat. Rev. Genet.* **19**, 518–529 (2018).
45. Spector, D. H. & Baltimore, D. Polyadenylic acid on poliovirus RNA: IV. Poly(U) in replicative intermediate and double-stranded RNA. *Virology* **67**, 498–505 (1975).
46. Steil, B. P., Kempf, B. J. & Barton, D. J. Poly(A) at the 3′ End of Positive-Strand RNA and VPg-Linked Poly(U) at the 5′ End of Negative-Strand RNA Are Reciprocal Templates during Replication of Poliovirus RNA. *J. Virol.* **84**, 2843–2858 (2010).
47. Kempf, B. J., Kelly, M. M., Springer, C. L., Peersen, O. B. & Barton, D. J. Structural features of a picornavirus polymerase involved in the polyadenylation of viral RNA. *J. Virol.* **87**, 5629–5644 (2013).
48. Nousch, M., Yeroslaviz, A., Habermann, B. & Eckmann, C. R. The cytoplasmic poly(A) polymerases GLD-2 and GLD-4 promote general gene expression via distinct mechanisms. *Nucleic Acids Res.* **42**, 11622–11633 (2014).

49. Lloyd, R. E. Nuclear proteins hijacked by mammalian cytoplasmic plus strand RNA viruses. *Virology* **479–480**, 457–474 (2015).
50. Nagy, P. D. & Pogany, J. The dependence of viral RNA replication on co-opted host factors. *Nat. Rev. Microbiol.* **10**, 137–149 (2011).
51. Rall, L. B., Standring, D. N., Laub, O. & Rutter, W. J. Transcription of hepatitis B virus by RNA polymerase II. *Mol. Cell. Biol.* **3**, 1766–1773 (1983).
52. Seeger, C. & Mason, W. S. Molecular biology of hepatitis B virus infection. *Virology* **479–480**, 672–686 (2015).
53. Ko, C. *et al.* Hepatitis B virus genome recycling and de novo secondary infection events maintain stable cccDNA levels. *J. Hepatol.* **69**, 1231–1241 (2018).
54. Ladner, S. K. *et al.* Inducible expression of human hepatitis B virus (HBV) in stably transfected hepatoblastoma cells: a novel system for screening potential inhibitors of HBV replication. *Antimicrob. Agents Chemother.* **41**, 1715–1720 (1997).
55. Rivera-Serrano, E. E., González-López, O., Das, A. & Lemon, S. M. Cellular entry and uncoating of naked and quasi-enveloped human hepatoviruses. *eLife* **8**, e43983 (2019).
56. Shukla, P. *et al.* Adaptation of a genotype 3 hepatitis E virus to efficient growth in cell culture depends on an inserted human gene segment acquired by recombination. *J. Virol.* **86**, 5697–5707 (2012).
57. Luo, B. *et al.* Highly parallel identification of essential genes in cancer cells. *Proc. Natl. Acad. Sci. U. S. A.* **105**, 20380–20385 (2008).
58. Li, W. *et al.* MAGeCK enables robust identification of essential genes from genome-scale CRISPR/Cas9 knockout screens. *Genome Biol.* **15**, 554 (2014).
59. Eden, E., Navon, R., Steinfeld, I., Lipson, D. & Yakhini, Z. GOrilla: a tool for discovery and visualization of enriched GO terms in ranked gene lists. *BMC Bioinformatics* **10**, 48 (2009).
60. González-López, O. *et al.* Redundant Late Domain Functions of Tandem VP2 YPX3L Motifs in Nonlytic Cellular Egress of Quasi-enveloped Hepatitis A Virus. *J. Virol.* **92**, (2018).
61. Huch, M. *et al.* Long-term culture of genome-stable bipotent stem cells from adult human liver. *Cell* **160**, 299–312 (2015).